DOI: 10.61782/fa.2025.0593

FORUM ACUSTICUM EURONOISE 2025

MULTI-RESONANT MATERIAL BASED ON CHANNELS WITH CONTRASTING TORTUOSITY

Tomasz G. Zieliński*
Institute of Fundamental Technological Research
Polish Academy of Sciences
ul. Pawińskiego 5B, 02-106 Warsaw, Poland

Marie-Annick Galland
Ecole Centrale de Lyon, CNRS
UCB Lyon 1, INSA Lyon, LMFA, UMR 5509
Ecully, France

ABSTRACT

The paper presents theoretical and experimental studies on the original multi-resonant sound-absorbing material. A representative geometry of the material contains several channels (disjoint pore networks) of contrasting tortuosity. For the assumed material thickness, one can estimate the quarter-wavelength resonance frequency of each channel based on its tortuosity. The proposed estimate is sufficiently accurate or can be systematically adjusted to eliminate the predictable error. It can therefore be used to design a very effective sound-absorbing layer by tuning the resonance frequencies. This is because the sound absorption peaks for such a layer backed by a rigid wall occur at the resonant frequencies. The tuning is performed by tailoring the shape of the channels to obtain contrasting tortuosities that should distribute their corresponding resonant frequencies over the desired, wide frequency range. In this way, broadband absorption can be achieved. An additional goal of tailoring the channels is to fit them tightly inside the representative space of the material while maintaining their separation. In the proposed material design, all shapes and characteristic sizes are suitable for additive manufacturing, so a sample of the material was 3D printed. It was tested in an impedance tube for sound absorption to validate the theoretical results.

Keywords: *sound absorption, separated pore networks, quarter-wavelength resonances, acoustic metamaterials.*

**Corresponding author*: *tzielins@ippt.pan.pl.*

1. INTRODUCTION

Conventional acoustic materials such as open-cell foams, felts, wools and other high-porosity fibrous materials are good sound absorbers, but only in the medium and high frequency range if their thickness is limited to a few centimetres. Broadband sound absorption, including lower frequencies, can be achieved by using very thick layers or almost equally thick multilayer arrangements of such materials [1]. Significant or even perfect sound absorption at individual lower frequencies can be obtained with tuned designs of Helmholtz resonators [2] or micro-perforated plates backed by air cavities with optimised depths [3]. However, these solutions are narrowband and their classical forms are bulky.

Desired sub-wavelength performance, i.e. significant attenuation of low-frequency sound waves by acoustic layers thinner than the wavelength in air, can be achieved using various recently-developed architected acoustic materials and metamaterials [4]. Such acoustic treatments are based on: coiled-up cavities of various geometries [5–8] often covered by micro-perforated plates, labyrinthine channels [9–12], coiled Helmholtz resonators [13], etc. Their performance is typically narrowband. To solve this problem, various multi-resonant solutions enabling broadband absorption of low-frequency sound have been recently proposed and intensively investigated. Representative examples are: parallel assemblies of coiled-up [14,15] or spiral cavities [16], nested networks [17], parallel or nested arrangements of Helmholtz resonators [18, 19].

This work presents a multi-resonant sound-absorbing material based on carefully designed, separated channels. Their shapes are tailored to ensure contrasting tortuosities and fit well into the limited space of the material without overlapping. By increasing (decreasing) the tortuosity, the

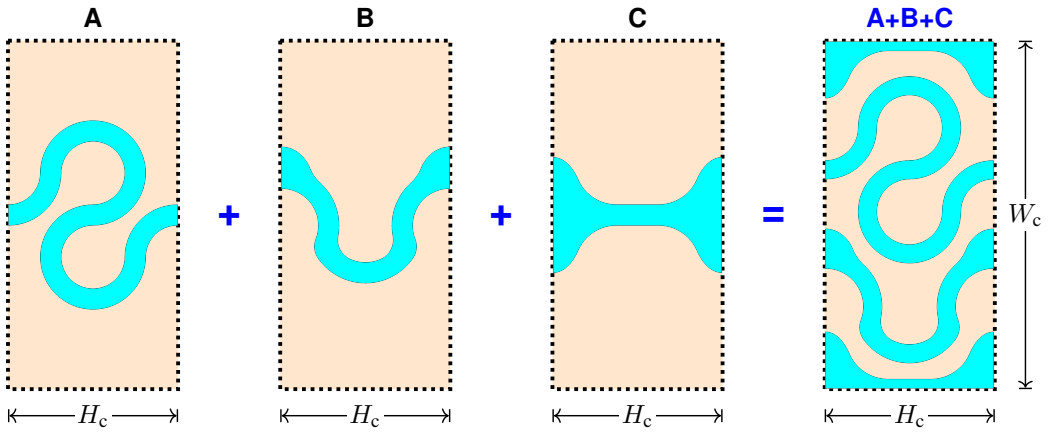

Figure 1. Periodic representative cells for three porous materials, each having a different pore network (A, B, or C), and for a multi-resonant material combining these three networks while keeping them separate.

associated quarter-wavelength resonance can be shifted to the desired lower (higher) frequency [20]. In this way, the resonances are spread over the required frequency range, which ensures broadband operation.

The outline of this paper is as follows. The tortuosity-based design of a multi-resonant material with three separated open-pore networks is discussed in Section 2.1. The main formulas necessary to model sound wave propagation and absorption in such materials are provided in Sections 2.2 and 2.3. Section 3.1 presents a 3D printed sample of the multi-resonant material and its testing configuration. The calculated and measured results of sound absorption by the multi-resonant material are confronted and discussed in Section 3.2. The main findings and conclusions are summarised is Section 4.

2. MATERIAL DESIGN AND MODELLING

2.1 Open-pore networks: designs based on tortuosity

Figure 1 shows four representative cells of periodic porous materials with an essentially two-dimensional structure. All cells are rectangular and have the same dimensions $W_c \times H_c = 16.5\,\text{mm} \times 8\,\text{mm}$. Each of the first three cells contains an open-pore network in the form of a single channel with a carefully designed shape. These networks and consequently the periodic cells and porous materials based on them will be referred to as network, cell or material A, B, and C.

The three networks were designed with the following two objectives in mind:

1. each network should have a designed tortuosity that is significantly different from the tortuosities of other pore networks to ensure different, desired quarter-wavelength resonance frequencies for a material layer of a specified, required thickness;

2. the network shapes should allow for a relatively tight fit within the limited space of a rectangular cell such that all the networks remain separated (i.e. do not overlap and ensure the required wall thickness between them) while providing the highest possible total porosity.

The realisation of the second objective resulted in the construction of the fourth representative cell shown in Figure 1, i.e. the periodic cell with three separated networks A+B+C. The total porosity of this cell (and of a periodic porous material composed of such cells) is the sum of the porosities of the three cells with one network, namely

$$\phi = \phi_A + \phi_B + \phi_C = 42.61\% \,. \tag{1}$$

Here and further in this work, ϕ_N (for N = A, B, and C) denotes the porosity of the periodic cell with a single open-pore network N. The values of these porosities are listed in Table 1.

As part of the design process to achieve the first objective, the Laplace problem for potential, i.e. inviscid flow was solved for each network N = A, B, C, to determine its kinematic tortuosity $\alpha_{\infty N}$ [21, 22]. The calculations were repeated every time the shape of the network was

Table 1. Main design parameters established for the designed networks and periodic representative cells, as well as the estimated and exact values (along with the estimation error) of the quarter-wavelength resonance (QWR) frequencies of the corresponding material layers with thickness $H = 40\,\text{mm}$.

Network N	Porosity ϕ_N [%]	Tortuosity $\alpha_{\infty N}$	QWR frequency* $\widetilde{f}_N$ [Hz]	f_N [Hz]	QWR est. error $\frac{\widetilde{f}_N - f_N}{f_N}$ [%]
A	17.14	9.71	694	645	7.60
B	11.43	3.33	1186	1126	5.33
C	14.04	1.69	1663	1610	3.29

*for $H = 40\,\text{mm}$

modified to tune its resonant behaviour, which was particularly the case for network B. The final tortuosity values are given in Table 1. It should be noted that they are very different from each other and as intended

$$\alpha_{\infty\text{A}} > \alpha_{\infty\text{B}} > \alpha_{\infty\text{C}}\,. \tag{2}$$

One should also notice that $\alpha_{\infty\text{A}}$ is much larger than the tortuosty of any conventional acoustic materials. Moreover, the geometric estimation of this tortuosity is possible and very accurate because network A is a narrow channel with constant width.

The proposed design method based on tortuosity was applied for each of the three networks to tune the respective quarter-wavelength resonance (QWR) frequency f_N of a porous layer with network N and thickness $H = 5H_\text{c} = 40\,\text{mm}$, i.e. containing five periodic cells per layer thickness. This is because, when the network tortuosity $\alpha_{\infty N}$ is known, the QWR frequency can be easily estimated by the upper-limit value $\widetilde{f}_N$, namely

$$f_N < \widetilde{f}_N = \frac{c_0}{4H\sqrt{\alpha_{\infty N}}}. \tag{3}$$

Here, c_0 is the speed of sound in air. The approach was simultaneously applied for all networks $N = \text{A}, \text{B}, \text{and C}$, to distribute the QWR frequencies more or less evenly over the desired frequency range. The upper estimates $\widetilde{f}_N$, listed in Table 1, prove to be very useful for this purpose.

2.2 Equivalent fluid model for sound-absorbing rigid-frame porous materials

The modelling of a multi-resonant acoustic material with multiple separated pore networks is based on the classical model of a porous material with a rigid frame and a single open-pore network. Time-harmonic wave propagation in such materials, with respect to the angular frequency $\omega = 2\pi f$ (f is the ordinary frequency), is determined by solving the Helmholtz equation of linear acoustics. For this purpose, it is first necessary to calculate the effective properties of the porous material modelled as an equivalent fluid, in particular, the effective speed of sound.

Homogenisation by the multi-scale asymptotic method (MAM) [23, 24] results in that the viscous and thermal effects are uncoupled at the micro-scale and the effective properties of a porous material depend on two dynamic permeabilities: one is related to the viscous oscillatory flow through a porous material and the other to the thermal diffusion in the pores. The dynamic viscous permeability $\mathcal{K}_N$ depends, in particular, on the kinematic viscosity ν of the air saturating the pores, while the dynamic thermal permeability Θ_N depends on the the thermal diffusivity of air ν'. Both are complex and frequency dependent functions that can be calculated using the well-known Johnson-Champoux-Allard-Lafarge-Pride (JCALP) model. The JACLP scaling functions depend on macro-parameters related to the structural geometry and static transport properties of the porous material. Therefore, for each porous material N, i.e. each periodic material with an open-pore network $N = \text{A}, \text{B}, \text{or C}$, the dynamic permeabilities are functions of the following parameters

$$\mathcal{K}_N = \mathcal{K}_N(\omega, \nu, \phi_N, \mathcal{K}_{0N}, \Lambda_N, \alpha_{0N}, \alpha_{\infty N}), \tag{4}$$

$$\Theta_N = \Theta_N(\omega, \nu', \phi_N, \Theta_{0N}, \Lambda'_N, \alpha'_{0N}). \tag{5}$$

See Refs. [1, 22] for the actual formulae of the JCALP model. Here, the porosity ϕ_N and the thermal charac-

teristic length Λ'_N are calculated from the geometry of the representative cell with network N, while the viscous characteristic length Λ'_N is determined from the aforementioned Laplace problem that is solved to calculate the kinematic tortuosity $\alpha_{\infty N}$. The static viscous permeability $\mathcal{K}_{0N}$ and the static viscous tortuosity α_{0N} are calculated from the solution of the Stokes flow through the periodic cell with network N, while the static thermal permeability Θ_{0N} and the static thermal tortuosity α'_{0N} are calculated from the solution of the Poisson problem defined on this periodic cell. See Refs. [21, 22, 24] for the details.

The dynamic permeabilities are used to calculate the effective density ϱ_N and the effective compressibility $\mathcal{C}_N$ for each material N, namely

$$\varrho_N = \frac{\nu \varrho_0}{\mathrm{i}\omega \mathcal{K}_N}, \quad \mathcal{C}_N = \frac{\phi_N}{P_0}\left(1 - \frac{\gamma - 1}{\gamma}\frac{\Theta_N}{\phi_N}\frac{\mathrm{i}\omega}{\nu'}\right). \quad (6)$$

where ϱ_0 and γ are the density and adiabatic index of air, respectively, P_0 is the ambient mean pressure, and i is the imaginary unit. Now, the effective speed of sound c_N, the effective wave number k_N, and the effective characteristic impedance Z_N can be calculated as follows

$$c_N = \frac{1}{\sqrt{\varrho_N \mathcal{C}_N}}, \quad k_N = \frac{\omega}{c_N}, \quad Z_N = \varrho_N c_N. \quad (7)$$

Note that not only the wave number but all effective properties are frequency dependent. In particular, $c_N = c_N(f)$ describes the dispersion in a porous material.

The QWR frequency f_N for a porous layer of thickness H can be determined by solving the following nonlinear equation

$$\frac{\mathrm{Re}\, c_N(f_N)}{4 f_N} = H, \quad (8)$$

where the real part of the effective speed of sound defines the acoustic wave velocity in the porous medium. Equation (8) was solved for the three materials N = A, B and C, assuming in each case the same layer thickness $H = 40\,\mathrm{mm}$. The resulting resonance frequencies f_N are compared in Table 1 with their upper-limit estimates $\widetilde{f}_N$, proving that the estimates are quite accurate. The typical expected accuracy is indicated by the relative errors shown in the last column of Table 1.

The surface acoustic impedance is an important acoustic indicator for sound absorbing and isolating materials. For a layer of porous material N and thickness H, it is calculated as

$$\mathcal{Z}_{\mathrm{s}N} = Z_N \coth(\mathrm{i}k_N H)\,. \quad (9)$$

It can be used to calculate other acoustic indicators such as the reflection coefficient $\mathcal{R}_N$ and the sound absorption coefficient $\mathcal{A}_N$, namely

$$\mathcal{R}_N = \frac{\mathcal{Z}_{\mathrm{s}N} - Z_0}{\mathcal{Z}_{\mathrm{s}N} + Z_0}, \quad \mathcal{A}_N = 1 - \left|\mathcal{R}_N\right|^2. \quad (10)$$

Here, $Z_0 = \varrho_0 c_0$ is the characteristic impedance of air.

2.3 Material with multiple, separated pore networks

The material with multiple open-pore networks that are separated from each other can be considered as an assembly of the corresponding single-network materials arranged in parallel, or rather independently occupying the same geometric space. Consequently, in the example investigated in this work, the triple-network periodic material marked as A+B+C (see Figure 1) can be modelled with three effective fluids that are acoustically equivalent to porous materials A, B and C, respectively. These equivalent fluids share the same computational domain, but the wave propagation in each of them is governed by an independent Helmholtz equation. There are therefore three acoustic pressures that are not coupled *within* the computational domain. However, they are coupled – which usually means that they are equalised – on some (or all) of its boundaries, so that wave propagation in the equivalent fluids corresponding to the individual networks is not completely independent. In the case when a layer of the material with multiple, separated networks is backed by a rigid wall, the coupling, i.e. pressure equalisation, occurs only on the front surface of the layer. It is easy to show that the surface acoustic impedance for such a hard-backed layer equals

$$\mathcal{Z}_{\mathrm{s}} = \frac{1}{\sum\limits_{N=\mathrm{A,B,C}} \mathcal{Z}_{\mathrm{s}N}^{-1}} = \frac{1}{1/\mathcal{Z}_{\mathrm{sA}} + 1/\mathcal{Z}_{\mathrm{sB}} + 1/\mathcal{Z}_{\mathrm{sC}}}. \quad (11)$$

This is the classic result for the impedance of a system of components N = A, B, C, set in parallel. It should be noted that the situation becomes much more complicated and dramatically different when the layer is supported by even a very thin air gap and not directly by a rigid wall. This is because in such a case the pressures in all networks also equalise on the back surface of the porous layer. Consequently, determining the surface acoustic impedance requires in this case much more complex calculations [25].

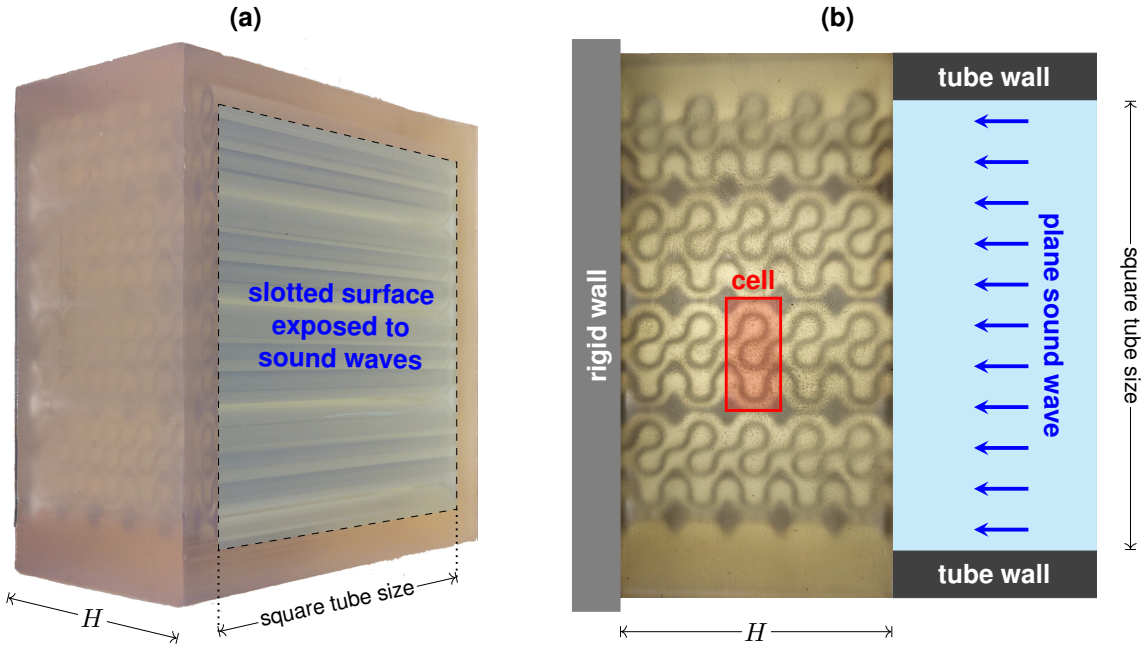

Figure 2. 3D printed sample of the multi-resonant material with three separated pore networks: (a) general view, (b) side view showing all pore networks (due to sample transparency) with one representative cell marked with a red rectangle. In the side view, the sample is placed inside the measurement scheme showing a fragment of a square impedance tube and a plane acoustic wave at normal incidence to the sample surface.

When the surface acoustic impedance $\mathcal{Z}_s$ is determined for the hard-backed multi-resonant material using Equation (11), the corresponding reflection coefficient $\mathcal{R}$ as well as the coefficient of sound absorption $\mathcal{A}$ are calculated using standard formulae, namely

$$\mathcal{R} = \frac{\mathcal{Z}_s - Z_0}{\mathcal{Z}_s + Z_0}, \quad \mathcal{A} = 1 - \left|\mathcal{R}\right|^2. \tag{12}$$

3. PROTOTYPING, TESTING AND VALIDATION OF MULTI-RESONANT MATERIAL

3.1 3D printed sample

Figure 2 (a) shows an additively manufactured sample of the designed multi-resonant material. The sample has a cuboid shape with a square base. Its thickness (height) is $H = 40$ mm. There are twelve slits on the front surface of the sample that lead to (four triplets of) separate networks. The corresponding twelve exit slits on the back side of the sample were sealed with an aluminium tape to prevent sound leakages when the sample was backed by a rigid wall and tested in a 66 mm square impedance tube. The testing configuration is depicted in Figure 2 (b).

The sample was 3D printed in the stereolithography (SLA) technology using a photopolymer resin of low viscosity so that its residues could be removed even from the most tortuous of the network channels. The resin is transparent, so that all the separate networks of the material can be seen in the photograph of one side of the sample shown in Figure 2 (b). The rectangular periodic cell is marked in red in this photograph, mirroring the design labelled as A+B+C in Figure 1. One should notice that there are five such cells per sample thickness. The configuration scheme shown in Figure 2 (b) illustrates how the sample is backed by a rigid wall and impinged at the front by a plane acoustic wave propagating in a square impedance tube.

3.2 Sound absorption: predictions and measurements

The modelling discussed in Section 2 was applied to predict the sound absorption by different material layers in a

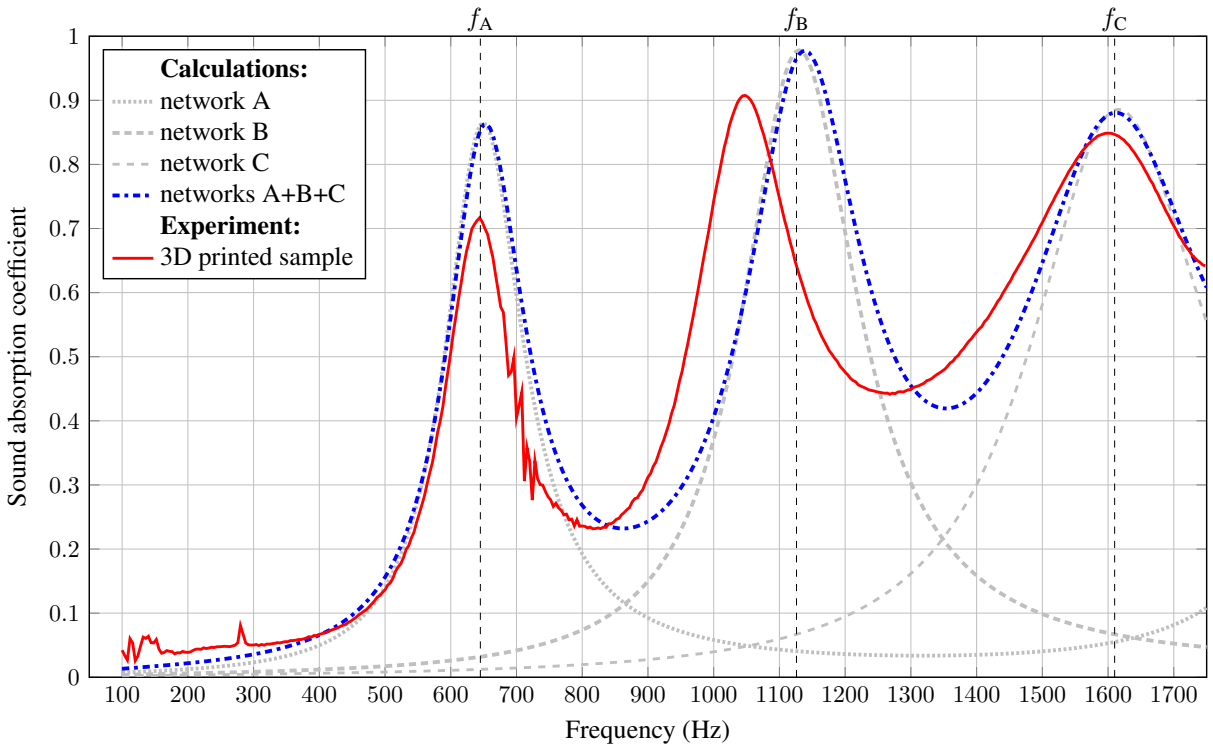

Figure 3. Sound absorption measured for a 3D printed sample of the mutli-resonant material with three pore networks (red curve) compared with the corresponding prediction (blue curve) and with the sound absorption curves calculated for single-network layers (grey curves) of the same thickness.

configuration where the layer under consideration is supported by a rigid wall, as illustrated in Figure 2 (b) for the 3D printed sample. Each material is based on one of the four periodic representative cells shown in Figure 1, which gives the four following cases:

1. a hard-backed porous layer with network A,
2. a hard-backed porous layer with network B,
3. a hard-backed porous layer with network C,
4. a hard-backed porous layer with three separated networks, arranged as in cell A+B+C, see Figure 1.

Each layer has five identical periodic cells along its thickness, which is therefore the same, i.e. $H = 40$ mm, as in the case of the 3D printed sample.

To predict sound absorption by hard-backed layers, the macro-parameters mentioned in Section 2.2 were first calculated for each of the three periodic cells with a single pore network N = A, B, C. In each case, the cell geometry used for calculations was *not exactly* the same as that used to 3D print the sample. However, the necessary geometric modification was minor and generally consisted of reducing the channel width by 0.1 mm to match the actual width of 3D printed channels. Incidentally, the values given in Table 1 were determined for such updated cell geometries. The macro-parameters were used to calculate the effective properties. Then, the sound absorption of each single-network layer was calculated using formulae (9) and (10). Equations (11) and (12) were used to calculate the sound absorption for the layer with three separated networks.

Sound absorption curves determined for the four materials are compared in Figure 3 within the frequency range up to 1.75 kHz. It should be observed that the absorption peak for the hard-backed layer with network A is almost at $f_A = 645$ Hz, which is the QWR frequency predicted for this layer by Equation (8). Similarly, the absorp-

tion peaks for the layer with network B and the layer with network C are close to their respective QWR frequencies. The sound absorption curve marked in blue was calculated for the layer with three separated networks A+B+C. It envelopes the three (grey) curves determined for the single-network layers. This curve envelope closely adheres to the absorption peaks, but not between them, where the sound absorption of the layer with three separate networks is noticeably higher than that of any single-network layer.

The blue sound absorption curve clearly demonstrates the multi-resonant acoustic behaviour of the material with multiple networks. This is confirmed by the experimental results, i.e. the red sound absorption curve in Figure 3, measured in an impedance tube for the 3D printed sample. Discrepancies between calculations and measurements are due to printing imperfections. They should be related to the geometric quality of each 3D printed network. It seems that the shape of the printed network B differs, albeit slightly but significantly, from the shape used to calculate its corresponding macro-parameters. One can expect that the actual tortuosity in this case is slightly larger than the calculated value, because the absorption peak associated with this network occurs at a frequency that is about 80 Hz lower than the predicted value of $f_B = 1126$ Hz.

4. CONCLUSIONS

Broadband low-frequency sound absorption can be achieved by porous materials with separate channels of contrasting tortuosity. Such materials exhibit multi-resonant behaviour and the individual resonant frequencies can be tuned during the design process to the desired values. To ensure overall broadband performance, they should be evenly distributed over the entire frequency range of interest.

In the proposed material design procedure, the main tailoring parameter is the tortuosity of each channel. Knowing this parameter and the material thickness, the quarter-wavelength resonance frequency associated with a given channel can be quickly estimated with acceptable accuracy. In the design process, this resonance can be shifted towards a lower frequency by increasing the tortuosity [20]. Even for a relatively thin material, this can be a very low frequency indeed, provided that the channel tortuosity is sufficiently high.

The design procedure is very efficient, especially for narrow channels of constant width because their tortuosity can be determined analytically with high accuracy based on the channel length [12, 26, 27]. Channel shapes should be designed simultaneously or at least taking into account the already constructed channels. This is because their tortuosities should be significantly different, and moreover, all channels should fit into the material space without overlapping but at the same time allow for the highest possible porosity. Optimised, three-dimensional design of channel shapes should lead to the creation of thin but very efficient and broadband, multi-resonant materials of this type.

5. ACKNOWLEDGMENTS

This research was financially supported by the National Science Centre (NCN), Poland, under Grant Agreement No. 2021/41/B/ST8/04492.

6. REFERENCES

[1] J. F. Allard and N. Atalla, *Propagation of Sound in Porous Media: Modeling Sound Absorbing Materials, 2nd ed.* Chichester: John Wiley & Sons, 2009.

[2] D. T. Blackstock, *Fundamentals of physical acoustics*. New York: Wiley, 2000.

[3] M. Yairi, K. Sakagami, K. Takebayashi, and M. Morimoto, "Excess sound absorption at normal incidence by two microperforated panel absorbers with different impedance," *Acoustical Science and Technology*, vol. 32, no. 5, pp. 194–200, 2011.

[4] J.-P. Groby, N. Jiménez, and V. Romero-García, "Acoustic metamaterial absorbers," in *Acoustic Waves in Periodic Structures, Metamaterials, and Porous Media: From Fundamentals to Industrial Applications* (N. Jiménez, O. Umnova, and J.-P. Groby, eds.), ch. 5, pp. 167–204, Cham: Springer International Publishing, 2021.

[5] X. Cai, Q. Guo, G. Hu, and J. Yang, "Ultrathin low frequency sound absorbing panels based on coplanar spiral tubes or coplanar Helmholtz resonators," *Applied Physics Letters*, vol. 105, p. 121901, 2014.

[6] Y. Li and B. M. Assouar, "Acoustic metasurface-based perfect absorber with deep subwavelength thickness," *Applied Physics Letters*, vol. 108, p. 063502, 2016.

[7] Y. Wang, H. Zhao, H. Yang, J. Zhong, D. Zhao, Z. Lu, and J. Wen, "A tunable sound-absorbing metamaterial based on coiled-up space," *Journal of Applied Physics*, vol. 123, p. 185109, 2018.

[8] G. Catapane, G. Petrone, O. Robin, and K. Verdière, "Coiled quarter wavelength resonators for low-frequency sound absorption under plane wave and diffuse acoustic field excitations," *Applied Acoustics*, vol. 209, p. 109402, 2023.

[9] K. Donda, Y. Zhu, S.-W. Fan, L. Cao, Y. Li, and B. Assouar, "Extreme low-frequency ultrathin acoustic absorbing metasurface," *Applied Physics Letters*, vol. 115, p. 173506, 2019.

[10] S. Kumar and H. P. Lee, "Labyrinthine acoustic metastructures enabling broadband sound absorption and ventilation," *Applied Physics Letters*, vol. 116, p. 134103, 2020.

[11] T. Yuan, X. Song, J. Xu, B. Pan, D. Sui, H. Xiao, and J. Zhou, "Tunable acoustic composite metasurface based porous material for broadband sound absorption," *Composite Structures*, vol. 298, p. 116014, 2022.

[12] T. G. Zieliński, K. C. Opiela, N. Dauchez, T. Boutin, M.-A. Galland, and K. Attenborough, "Extremely tortuous sound absorbers with labyrinthine channels in non-porous and microporous solid skeletons," *Applied Acoustics*, vol. 217, p. 109816, 2024.

[13] J.-S. Chen, Y.-B. Chen, Y.-H. Cheng, and L.-C. Chou, "A sound absorption panel containing coiled helmholtz resonators," *Physics Letters A*, vol. 384, no. 35, p. 126887, 2020.

[14] G. do N. Almeida, E. F. Vergara, L. R. Barbosa, and R. Brum, "Low-frequency sound absorption of a metamaterial with symmetrical-coiled-up spaces," *Applied Acoustics*, vol. 172, p. 107593, 2021.

[15] A. Magnani, C. Marescotti, and F. Pompoli, "Acoustic absorption modeling of single and multiple coiled-up resonators," *Applied Acoustics*, vol. 186, p. 108504, 2022.

[16] A. Carvalho de Sousa, E. Deckers, C. Claeys, and W. Desmet, "On the assembly of Archimedean spiral cavities for sound absorption applications: Design, optimization and experimental validation," *Mechanical Systems and Signal Processing*, vol. 147, p. 107102, 2021.

[17] A. Jamois, D. Dragna, T. G. Zieliński, and M.-A. Galland, "Acoustic absorption of 3D printed samples at normal incidence and as a duct liner," *Acta Acustica*, vol. 9, p. 12, 2025.

[18] X. Yang, X. Shen, F. Yang, Z. Yin, F. Yang, Q. Yang, C. Shen, M. Xu, and J. Wan, "Acoustic metamaterials of modular nested Helmholtz resonators with multiple tunable absorption peaks," *Applied Acoustics*, vol. 213, p. 109647, 2023.

[19] Z. Mei, Y. Lyu, X. Li, X. Cheng, and J. Yang, "Parallel-coupled hierarchical and reconfigurable structure for broadband sound absorption," *Applied Acoustics*, vol. 221, p. 109990, 2024.

[20] K. Attenborough, "Microstructures for lowering the quarter wavelength resonance frequency of a hard-backed rigid-porous layer," *Applied Acoustics*, vol. 130, pp. 188–194, 2018.

[21] C. Perrot, F. Chevillotte, and R. Panneton, "Bottom-up approach for microstructure optimization of sound absorbing materials," *The Journal of the Acoustical Society of America*, vol. 124, no. 2, pp. 940–948, 2008.

[22] T. G. Zieliński, R. Venegas, C. Perrot, M. Červenka, F. Chevillotte, and K. Attenborough, "Benchmarks for microstructure-based modelling of sound absorbing rigid-frame porous media," *Journal of Sound and Vibration*, vol. 483, p. 115441, 2020.

[23] E. Sanchez-Palencia, *Non-Homogenous Media and Vibration Theory*. Lecture Notes in Physics, Springer-Verlag, 1980.

[24] J.-L. Auriault, C. Boutin, and C. Geindreau, *Homogenization of Coupled Phenomena in Heterogenous Media*. ISTE Ltd., John Wiley & Sons, Inc., 2009.

[25] K. Verdière, R. Panneton, S. Elkoun, T. Dupont, and P. Leclaire, "Transfer matrix method applied to the parallel assembly of sound absorbing materials," *The Journal of the Acoustical Society of America*, vol. 134, pp. 4648–4658, 12 2013.

[26] K. Attenborough, "Macro- and micro-structure designs for porous sound absorbers," *Applied Acoustics*, vol. 145, pp. 349–357, 2019.

[27] B. Ghanbarian, A. G. Hunt, R. P. Ewing, and M. Sahimi, "Tortuosity in porous media: A critical review," *Soil Science Society of America Journal*, vol. 77, no. 5, pp. 1461–1477, 2013.